Journal of Molecular Structure 1322 (2025) 140267

Contents lists available at ScienceDirect

Journal of Molecular Structure

journal homepage: www.elsevier.com/locate/molstr

Structural, DNA/BSA binding interactions and cytotoxicity studies of carboxamide (pyridyl)pyrazine palladium(II) complexes

Sabathile T. Mvelase [a], Saheed O. Benson [b], Reinner O. Omondi [a], Robert T. Kumah [a], Amos A. Fatokun [b], Stephen O. Ojwach [a,*]

[a] School of Chemistry and Physics, University of KwaZulu-Natal, Private Bag X01, Scottsville, Pietermaritzburg 3201, South Africa
[b] Centre for Natural Products Discovery (CNPD), School of Pharmacy and Biomolecular Sciences, Faculty of Science, Liverpool John Moores University, Liverpool L3 3AF, UK

ARTICLE INFO

Keywords:
Palladium
Carboxamide
Structures
DNA binding
Cytotoxicity

ABSTRACT

Reactions of ligands [N^2, N^3-bis(pyridin-2-yl)pyrazine-2,3-dicarboxamide] (**L1**), [N^2, N^3-bis(6-methylpyridin-2-yl)pyrazine-2,3-dicarboxamide] (**L2**), [N^2,N^3-bis(4-methylpyridin-2-yl)pyrazine-2,3-dicarboxamide] (**L3**) and [N^2, N^3-bis(quinoline-8-yl)pyrazine-2,3-dicarboxamide] (**L4**) with [$PdCl_2(NCMe)_2$] afforded the respective palladium(II) complexes: [Pd_2(**L1**)$_2Cl_2$] **(Pd1)**, [Pd_2(**L2**)$_2Cl_2$] **(Pd2)**, [Pd_2(**L3**)$_2Cl_2$] **(Pd3)** and [Pd(**L4**)Cl] **(Pd4)**. Molecular structures of complexes **Pd1** and **Pd3** are dinuclear containing two bridging bidentate ligand units. The interactions of the palladium complexes (**Pd1**-**Pd4**) with calf thymus DNA (CT-DNA) were monitored using UV–Vis and fluorescence spectroscopy and revealed intercalative binding modes, with intrinsic binding constants (K_b) in the order of 10^6 M^{-1}. Bovine serum albumin (BSA) interaction was evaluated using fluorescence techniques and displayed a static quenching mechanism. The cytotoxic effects of the complexes **Pd1-Pd4** were examined against human breast cancer cell lines MCF-7 and MDA-MB-231, and human transformed lung cell line MRC5-SV2 (a model of lung cancer) and its parental normal lung fibroblast cell line MRC5. While the complexes **Pd1** and **Pd4** showed significant to moderate cytotoxicity against MCF-7 (IC_{50} of 11.2 μM and 61.5 μM, respectively), complexes **Pd2** and **Pd3** were inactive. All the complexes were inactive against the MDA-MB-231 cell line, and **Pd2-Pd4** were inactive against the MRC5-SV2 cell line. Compounds **Pd1** exhibited lower cytotoxicity against the normal cell line MRC5.

1. Introduction

Palladium(II) complexes have gained interest as promising anticancer agents due to their comparable chemical and coordination behaviour to platinum-based complexes [1–3]. To date, a number of palladium(II) complexes derived from different ligand backbones have been investigated as potential anti-cancer agents with varied outcomes [4–7]. Of these palladium(II) complexes, some have shown better cytotoxicity towards cancer cell lines together with better selectivity towards normal cell lines when compared to the well-established platinum-based cisplatin [8,9]. For example, the 1,2- and 1,4-diazine palladium(II) complexes demonstrated superior cytotoxicity (IC_{50} values of 5.4 μM and 6.9 μM) compared to cisplatin (IC_{50} value of 7.8 μM) against squamous cell carcinoma [10]. In another work, Wang and co-workers reported the cytotoxicity of a series of highly selective palladium(II) substituted-terpyridine complexes which shows better cytotoxic activity against cancer cell lines with IC_{50} values range of 0.2847–0.3897 μM, MCF-7; 0.7408–2.141 μM, A549; 1.273–1.927 μM, Eca-109; 0.4593–1.616 μM, Bel-7402 and normal cell line with IC_{50} >20 of all complexes [11].

Among the common ligands which have been used to synthesize and stabilize palladium(II) complexes are the amide ligands, either in their anionic or neutral forms [12]. The versatile coordination behaviour of these amide ligands; displaying either NˆN for anionic ligands and NˆO coordination in the neutral forms, makes them robust ligands for stabilization of a wide range of metal complexes for various applications [13–15]. For instance, van Rijt reported that Nˆ *N*-pH-picolinamide ruthenium(II) arene complexes display improved cytotoxicity in some cancer cells such as colon, ovarian, and cisplatin-resistant ovarian human cancer cell lines, whereas the analogous complexes with NˆO coordination of *N*-pH-picolinamide ruthenium(II) arene were inactive [16]. In separate reports, NˆN heterocyclic chelating ligands bearing

* Corresponding author.
E-mail address: ojwach@ukzn.ac.za (S.O. Ojwach).

https://doi.org/10.1016/j.molstruc.2024.140267
Received 22 July 2024; Received in revised form 25 September 2024; Accepted 1 October 2024
Available online 5 October 2024

pyridine, quinoline, and pyrazine motifs have been observed to exhibit anticancer activity [17–19]. For example, Zafar and the group studied *N*-(1-Alkylpyridin-4(*1H*)-ylidene) amide palladium(II) complex as a potential anti-cancer agents and recorded IC_{50} value of 21.3 μM against MCF-7 cancer cell lines [20]. In addition, Churusova and co-workers have reported that 2-methylsulfinyl-N-(quinolin-8-yl)acetamide palladium(II) complexes display IC_{50} value of 22 μM against HCT116 cancer cell line [21].

In the quest to design more effective metal-based anti-cancer drugs, a number of strategies have been employed to fine-tune the properties of these metal complexes. These include the design of planar molecules, more water-soluble (hydrophilic) complexes, and kinetically labile metal complexes among others [22]. Another strategy which has been adopted and is currently gaining significant attraction is the design of polynuclear complexes as potential anti-cancer agents. The assumption behind the development of polynuclear complexes anti-cancer drugs is that they may simultaneously interact with DNA at multiple sites which may thus lead to the limitations of severe side effects [23]. One such example is the report of Alisufi et al. [24] on DNA, bovine serum albumin (BSA) interactions and anti-cancer activity of dinuclear palladium (II) complex anchored on 1,4-phenylenediamine-bis-(chloroethylenediamine ligand. This dinuclear palladium complex exhibits enhanced cytotoxic activity of 17.03 μM against MOLT-4 cancer cells compared to the IC_{50} value of 33.3 μM recorded for the corresponding mononuclear $[Pd(Octyl\text{-}am)_2Cl_2]$ [25].

For the past years, our research has been working on the investigation of ruthenium(II) and palladium complexes, derived from various ligand motifs, as potential anti-cancer agents. In one such adventure, we recently reported the use of π-conjugated carboxamide mononuclear palladium(II) complexes as potential anti-cancer agents, with promising results. For example, the lead palladium complex in this series demonstrates IC_{50} values of 3.9 μM, 9.8 μM, 0.1 μM, 0.04 μM and 35.2 μM and SI of >2 against A549, Pc-3, HT-29, Caco-2 and HeLa cell lines [26], which are superior to these reported for the reference drug cisplatin. Motivated by these promising results, we aimed to further elucidate the possible effect of incorporating dinuclear metal cores using similar carboxamide ligands on the cytotoxicity of the resultant palladium(II) complexes. Thus herein, we report the syntheses and structural investigations of palladium(II) complexes supported on (pyridyl)pyrazine carboxamide ligands and their interactions with DNA/BSA biomolecules and their cytotoxicity against human breast cancer cell lines (MCF-7, and MDA-MB-231), transformed human foetal lung cell line (MRC5-SV2) – a model of lung cancer, as well as normal human foetal lung fibroblast cell line (MRC-5).

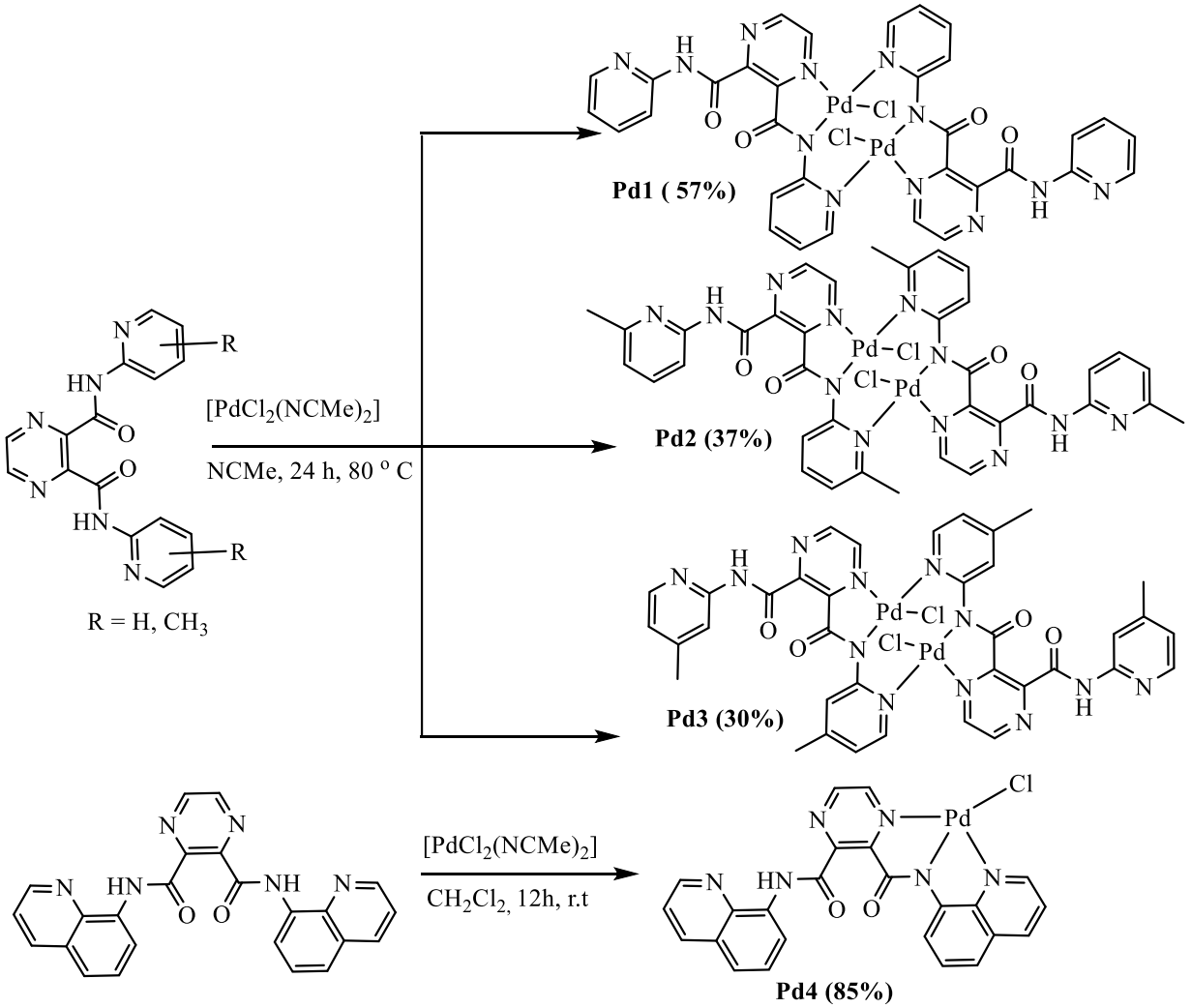

Scheme 1. Synthesis of mononuclear and dinuclear (pyridyl)pyrazine carboxamide palladium(II) complexes **Pd1-Pd4**.

2. Result and discussion

2.1. Synthesis and characterization of (pyridyl)pyrazine carboxamide ligands and their palladium(II) complexes

The pyrazine-2,3-dicarboxamide ligands; [N^2, N^3-bis(pyridin-2-yl) pyrazine-2,3-dicarboxamide] **(L1),** [N^2, N^3-bis(6-methylpyridin-2-yl) pyrazine-2,3-dicarboxamide] (**L2**), [N^2, N^3-bis(4-methylpyridin-2-yl) pyrazine-2,3-dicarboxamide] (**L3**), and [N^2, N^3-bis(quinoline-8-yl)pyrazine-2,3-dicarboxamide] (**L4**) were synthesized by following modified literature procedures [27,26]. Treatments of pyrazine-2,3- dicarboxylic acid with the respective amines in the presence of triphenylphosphite in pyridine resulted in the formation of compounds **L1-L4** in low to good yields (38–74 %) as depicted in **Scheme S1**. The respective dinuclear palladium(II) complexes **Pd1-Pd3** were prepared in low to moderate yields (30–63 %) from the reaction of respective dicarboxamide ligands with $PdCl_2(NCMe)_2$ in a 1:1 ratio in acetonitrile (Scheme 1). On the other hand, the mononuclear palladium(II) complex **Pd4** was prepared from the reactions of **L4** with equimolar amounts of $PdCl_2(NCMe)_2$ in good yields (74 %). The reaction of **L4** with $PdCl_2(NCMe)_2$ in a 1:2 mole ratio also resulted in the formation of the same mononuclear complex. Thus the formation of the mononuclear **Pd4** complex could be due to the NˆNˆN tridentate binding mode of **L4** as shown in Scheme 1.

The new compounds were characterized using ^{1}H NMR (**Figs. S1–S8**), ^{13}C NMR (**Figs. S9–S15**), FT-IR spectroscopy (**Figs. S16–S19**), mass spectrometry (**Figs. S20–S27**) and single crystal X-ray analysis for **Pd1** and **Pd3** (Figs. 1 and 2). While the ^{1}H NMR spectrum of **Pd3** (**Fig. S7**), showed a singlet assigned to the amidic proton N—H at 11.02 ppm with an integral value of 1, the ^{1}H NMR spectrum of the respective free ligand **L3** showed the N—H signal at 10.64 ppm with an integral value of 2 (**Fig. S3**). This is consistent with the deprotonation of one amidic N—H prior to complexation as depicted in Scheme 1 and the molecular structure of **Pd3** (Fig. 2). Similar observations were made in the ^{1}H NMR spectra of complexes **Pd1, Pd2** and **Pd4 (Figs. S1–S4)** and agree with literature findings for related carboxamide palladium(II) complexes [28]. In addition, two singlets of the pyrazine protons were observed in the ^{1}H NMR of the palladium(II) complexes. For example, in the ^{1}H NMR spectrum of **Pd3,** two signals at 9.09 and 9.12 ppm assigned to $H_{pyrazine}$ compared to the free ligand **L3** at 8.94 ppm.

^{13}C NMR data supported the trends and structures deduced from the ^{1}H NMR spectra of compounds. For example, in complex **Pd3**, two C=O peaks were observed at 163.3 and 166.92 ppm, which could be attributed to the non-coordinating arm of **L3 (Fig. S14)**. Similar signals were observed in ^{13}C NMR spectra of **Pd2** and **Pd4** (**Figs. S13** and **S15)** and agree with previous findings for related palladium(II) complexes [29, 26]. FT-IR spectral data was further employed in confirming the formation of the palladium(II) complexes **Pd1-Pd4**. For example, two C=O signals at 1632 cm^{-1} and 1705 cm^{-1} were observed in the FT-IR spectrum of complex **Pd3**, compared to one signal at 1682 cm^{-1} in the FT-IR spectrum of the respective ligand **L3** (**Fig. S18**). Similar trends in the FT-IR spectra were reported for related carboxamide metal complexes in literature [30–32]. Mass spectrometry (ESI-MS) proved to be useful in establishing the identity of the ligands and their respective palladium(II) complexes. All the palladium(II) complexes showed *m/z* signals that corresponded to their respective molecular ion or fragments. For example, the *m/z* peaks at 922.96 [M^+ +*H*] (**Pd1**), 1000.2 [M^+ +Na] (**Pd2**), 979.10 [M^++*H*] (**Pd3**), and 561 [M^+ +*H*] (**Pd4**) (**Figs. S20–S27**), were recorded. In addition, the good agreements between the calculated and experimental isotopic mass distributions of the complexes further ascertained their identity (**Figs. S24–S27**).

2.2. Molecular structures of complexes Pd1 and Pd3

Single crystals for **Pd1** and **Pd3** suitable for X-ray analysis were obtained from slow evaporation of DMSO solution at room temperature and used to confirm their solid-state structures. Figs. 1 and 2 show the solid-state structures and selected bond parameters of complexes **Pd1** and **Pd3** structures, while **Table S3** shows crystallographic data and structure refinement parameters of the compounds. Complexes **Pd1** and **Pd3** crystallize in orthorhombic and monoclinic systems with P-1, $P2_12_12$, and C2/c space groups, respectively. Complex **Pd1** crystallizes with two molecules of DMSO solvents in the lattice. In both palladium complexes (**Pd1** and **Pd3**), the coordination sphere consists of one bidentate ($N_{pyrazine}$ˆ N_{amide}) ligand and a second monodentate (N_{py}) ligand and one terminal *chlorido* ligand to complete the four-

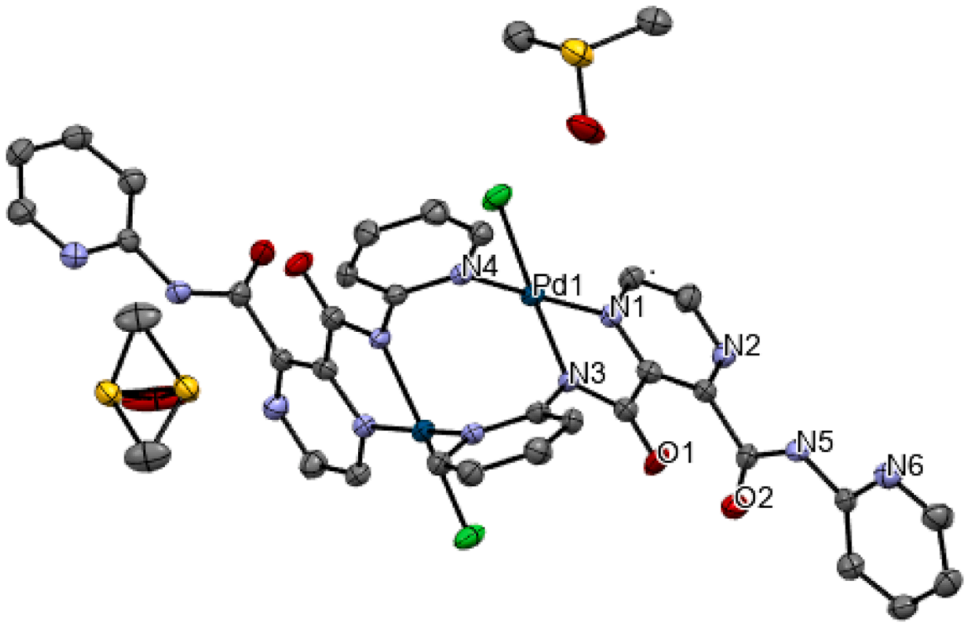

Fig. 1. Solid state structure of complex **Pd1**, drawn with 50 % probability ellipsoids. Hydrogen atoms were omitted for clarity. Selected bond lengths [Å]: Pd(1)-Cl (1), 2.2915(13); Pd(1)-N(4) 2.036(5); Pd(1)-N(1), 2.013(5); Pd(1)-N(3), 2.004(4). Selected bond angles []: N(3)-Pd(1)-Cl(1), 175.83(14); N(3)-Pd(1)-N(4), 95.88 (18); N(3)-Pd(1)-N(1), 80.29(18); N(4)-Pd(1)-Cl(1), 88.28(13); N(1)-Pd(1)-Cl(1), 95.58(13); N(1)-Pd(1)-N(4), 173.29(19).

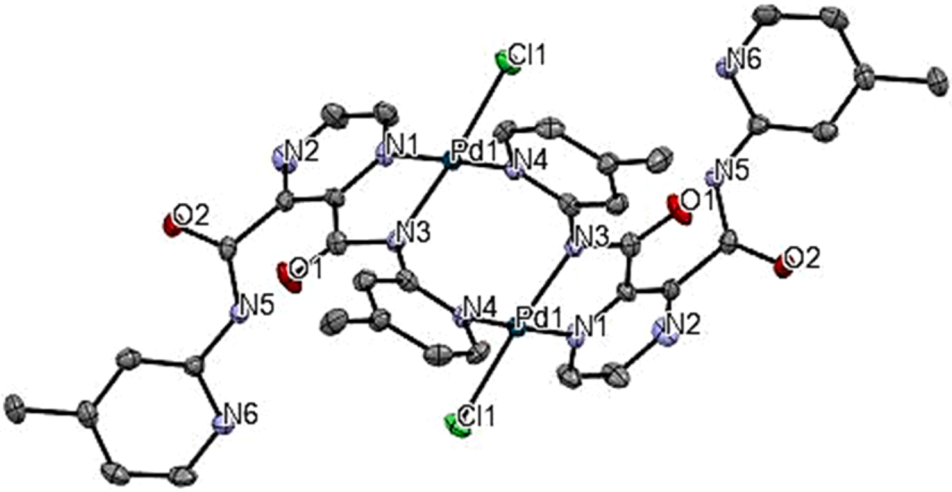

Fig. 2. Solid-state structure of **Pd3**, drawn with 50 % probability ellipsoids. Hydrogen atoms are omitted for clarity. Selected bond lengths [Å]: Pd(1)-Cl(1), 2.3154 (13); Pd(1)-N(3), 2.007(4); Pd(1)-N(1), 2.010(4); Pd(1)-N(41), 2.029(4). Selected bond angles [']: N(3)-Pd(1)-Cl(1), 174.65(13); N(3)-Pd(1)-N(4), 96.38(17); N(3)-Pd (1)-N(1), 80.68(17); N(4)-Pd(1)-Cl(1), 88.18(512; N(1)-Pd(1)-Cl(1), 94.65(13); N(1)-Pd(1)-N(4), 176.23(17).

coordination environment (Figs. 1 and 2). Thus, the structures consist of two anionic, two *chlorido* ligand units and metal atoms. Similar structures of related palladium(II) and zinc(II) complexes have been reported [33,34]. The bite angle for N1-Pd1-N3 of 80.68 ^{o} (17) in complex **Pd3** is comparable to the angle for N1-Pd1-N3 of 80.29 ^{o} (18) in complex **Pd1**, indicating little steric differences between the two ligands **L1** and **L3** respectively. Both angles in complexes **Pd1** and **Pd3** depart from 90 ^{o} consistent with slightly distorted square planar geomtries in both compounds. In addition, the bite angles 173.29 ^{o} (19) for **Pd1** and 176.23 ^{o} (17) for **Pd3** deviate from 180° to give distorted square planar geometries in both complexes in line with previous reports for similar carboxamide palladium(II) complexes [35,28,36].

Both complexes **Pd1** and **Pd3** generally exhibit comparable bond lengths. For instance, the Pd-N_{amide} bond lengths for **Pd1** of 2.004(4) Å and **Pd3** of 2.007(4) Å are comparable. The average Pd-N_{amide} bond lengths in **Pd1** and **Pd3** of 2.005 ± 0.0015 Å are within the maximum bond lengths of 2.001 Å Pd-N_{amide} reported for 16 related palladium(II) complexes containing similar Pd-N_{amide} bonds [37]. Similarly, the average bond length of Pd-N_{pyz} in complexes **Pd1** and **Pd3** of 2.011 ± 0.0021 Å is within the average bond length of 2.029 ± 12 Å obtained for 29 with similar bonds [31]. Additionally, the average Pd-N_{pyr} of **Pd1** and **Pd3** of 2.033 ± 0.0049 Å is comparable to the average bond distance of 2.032 ± 10 Å reported for 16 related compounds bearing similar Pd-N_{pyr} bonds [38]. The longer Pd-Cl bond length of 2.3154(13) Å in **Pd3** compared to Pd(1)-Cl(1) 2.2915(13) Å in complex **Pd1** could be ascribed to the stronger *trans*-effect induced by the presence of electron-donating methyl group in **L3.** Nonetheless, the Pd-Cl bond lengths of 2.304 ± 0.017 Å for compound complexes **Pd1** and **Pd3** are within the average Pd-Cl bond length of 2.326 ± 15 Å reported for 42 related complexes [39]. The differences in the C=O bond distances in the coordinated and non-coordinated ligand motifs; O1-C6; 1.238(6) Å and O2-C11; 1.222(7) Å (**Pd1)** as well as O1-C5; 1.234(7) Å and O2-C12; 1.240(7) Å (**Pd3)**, are in good agreement with the spectral data as previously discussed. The Pd-Pd- bond distance of 3.506 Å in complex **Pd3** is longer than that of complex **Pd1** 3.387 Å. This may be explained from the greater structural distortion in **Pd3** (due to the presence of methyl groups) compared to complex **Pd1** [40].

2.3. Stability studies of complexes Pd1 and Pd4 in aqueous media

Stability tests for complexes **Pd1** and **Pd4** were performed in both aqueous and DMSO media using ^{1}H NMR and UV–visible spectroscopies in order to assess their stability under biological conditions. ^{1}H NMR spectra of complexes **Pd1** and **Pd4** depicted in **Fig. S28**, showed no changes in the ligand proton signals of the complexes over the 48 h period. Similarly, the UV-visible spectra of complexes **Pd1** and **Pd4** in phosphate saline buffer (PBS) and DMSO conducted over a period of 48 h (**Figs. S29** and **S30**) remained invariant. Thus both the ^{1}H NMR and UV-visible spectral data were indicative of the stability of these complexes in biological media.

2.4. CT-DNA and BSA binding studies

2.4.1. CT-DNA UV–vis absorption spectral studies

DNA is known to be the main biological target in the treatment of cancer using metal-based drugs, thus understanding of the drug-DNA interactions is important in shedding some light on the mechanism of action of the given drug [41]. We thus studied the binding of the palladium(II) complexes (**Pd1-Pd4**) to CT-DNA duplex using electronic absorption spectroscopic titrations. Incremental addition of CT-DNA concentrations to fixed concentrations of the palladium(II) complexes resulted in a change in absorbance intensity (Figs. 3, **S31–33**). The spectral changes depicted hypochromic and bathochromic shifts upon increasing CT-DNA concentrations, which could be assigned to the π-π stacking of the palladium(II) complexes within the CT-DNA base pairs, indicating the existence of intercalation binding mode [42]. The intrinsic binding constant (K_b) values, 4.28–13.12 × 10^{6} M^{-1} for palladium (II) complexes **Pd1-Pd4** indicate strong interactions between the CT-DNA and the complexes. The binding constants follow the order **Pd3 > Pd2 > Pd1 > Pd4**. Negative values of Gibbs energy obtained suggest that the complexes interact with CT-DNA spontaneously [43, 44]. The obtained binding constants are comparable to other related palladium(II) complexes in literature with the same magnitude ((0.53–5.53) x10^{6} M^{-1}) and ((1.921–3.975) x10^{6} M^{-1}) [42,45].

2.4.2. Competitive CT-DNA ethidium fluorescence quenching studies

Ethidium bromide is a known strong DNA intercalating agent, usually used to probe the relative interactions of other compounds with DNA [46,47]. Thus, in this study, the interaction of the palladium(II) complexes (**Pd1-Pd4**) with CT-DNA was investigated by evaluating the fluorescence quenching experiments of the CT-DNA-EB complex in the presence of palladium(II) complexes (Figs. 4 **and S34–36**). For example, the spectral data using complex **Pd3** (Fig. 4), showed a hypochromic shift in fluorescence emission at 592 nm, which indicates that the complexes intercalate within CT-DNA base pairs to displace ethidium bromide. In addition, the emission intensity was quenched with a

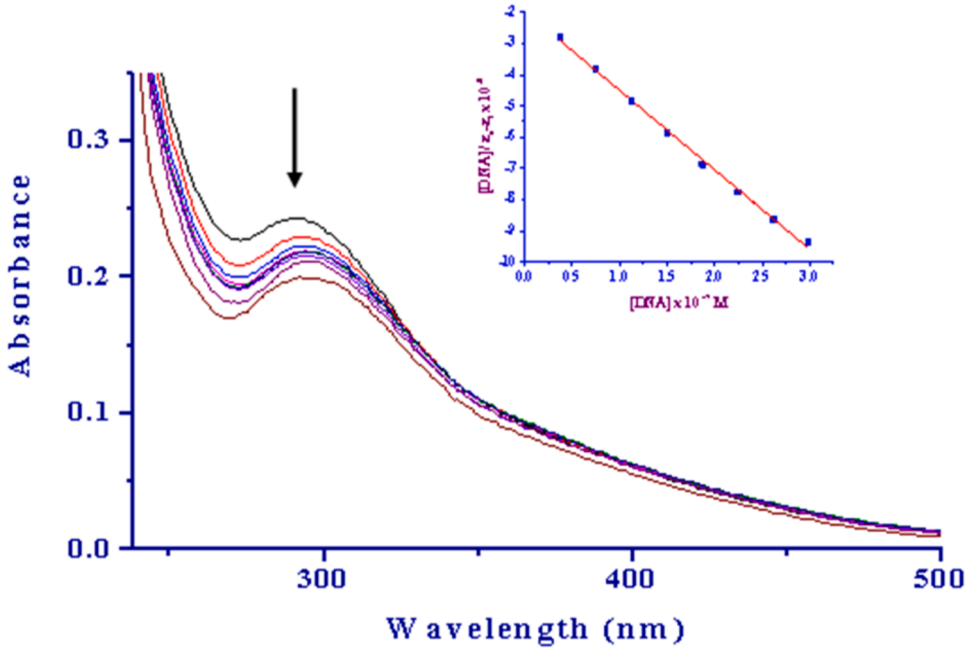

Fig. 3. Electronic absorption spectra of **Pd3** (25 μM) in 0.01 M PBS buffer at pH=7.4 upon addition of CT-DNA (0 - 16 μM). The arrow shows the decrease in absorbance upon the addition of increasing concentrations of CT-DNA. Inset is the linear plot of [CT-DNA] vs [DNA]/(ε_a-ε_f).

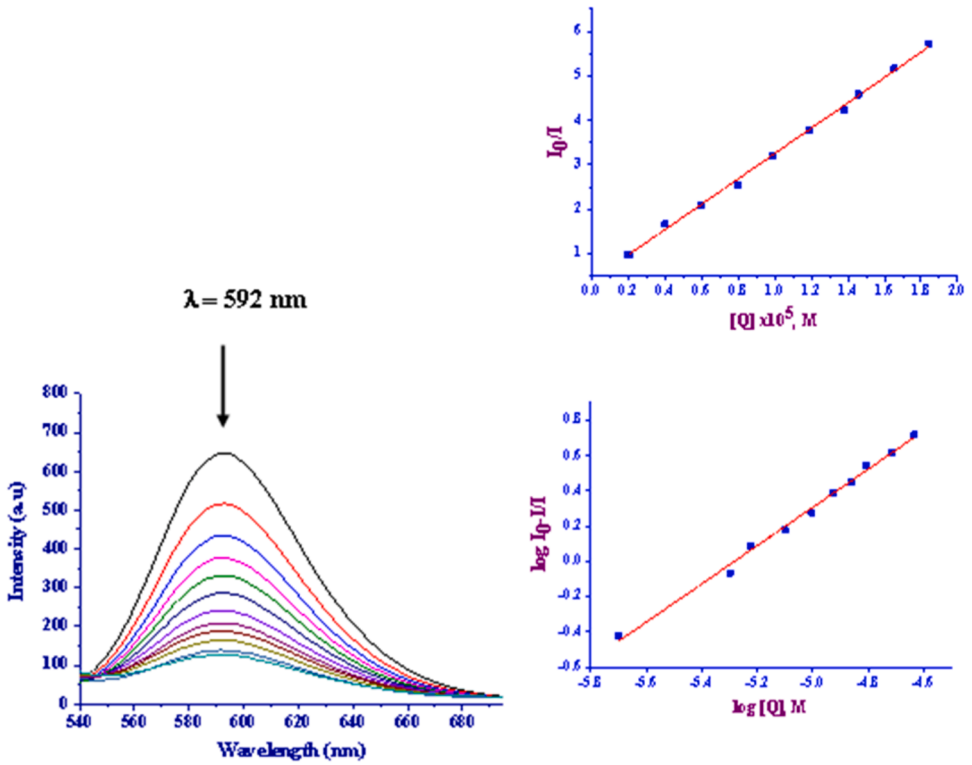

Fig. 4. Fluorescence emission spectra depicting the quenching upon addition of increasing amounts of **Pd3** to CT-DNA-EB: [EB] = 10 μM, [CT-DNA] = 10 μM. The arrow shows the intensity changes upon increasing the **Pd3** complex concentration. Inserted is the Stern-Volmer plot of I_o/I vs [Q] and Scatchard plot of log[(I_o–I)/I] vs log[Q].

notable red shift in all the spectra of the complexes (**Figs. S34–36**), which points to the existence of strong interactions between the palladium(II) complex and CT-DNA [48].

The Stern-Volmer quenching and biomolecular quenching rate constants for the interactions between the palladium(II) complexes (**Pd1-Pd4**) complexes and EB-CT-DNA were calculated by fitting the data to the Stern-Volmer equation ($I_o/I = 1 + K_{sv}[Q] = 1 + k_q\tau_0[Q]$). K_{sv} values in the range 1.82–28.41 $\times$ 10^5 M^{-1} were indicative that the complexes intercalate to the DNA to replace ethidium bromide dye. However, the magnitudes of observed K_{app} (3.93–25.02) x10^6 M^{-1} for complexes **Pd1-Pd4** are lower than the binding constants (10^7 M^{-1}) for classical intercalators and metallointercalators, thus indicating that the complexes

intercalate weakly to the DNA base pairs [49,50]. In general, a dynamic quenching mechanism is signified by values lower than those of strong biopolymer fluorescence quenchers (2×10^{10} $M^{-1}s^{-1}$) [51]. Therefore, the high bimolecular quenching rate constant k_q values (1.00–12.33) x10^{12} $M^{-1}s^{-1}$ reported for complexes **Pd1-Pd4** (Table 1) point to the displacement of ethidium bromide *via* the static mechanism [52]. The binding constants (K_F) and the number of binding sites (n) obtained from the linear plot of the Scatchard equation ($\log(I_o - I) / I = \log K_F + n \log [Q]$) are given in Table 1. The *n*-values (0.75–1.08) obtained were approximately equal to one, suggesting that the palladium complexes bind to a single site in the CT-DNA. It is important to note that the binding constants K_F (1.01–53.44) x10^4 M^{-1} support intercalative binding mode between palladium(II) complexes and CT-DNA-EB and is consistent with the bimolecular quenching rate constant (k_q). The binding constants of the complexes follow the order **Pd3 > Pd2 > Pd1 > Pd4**. From this trend, while it is not clear to us why the methyl substituted complexes (**Pd3** and **Pd2**) showed better binding interactions, it appears that the dinuclear complexes **Pd1-Pd3** showed higher binding constants compared to the mononuclear **Pd4**. This can be attributed to the increased electrostatic interactions between the DNA and the two palladium atoms in the dinuclear complexes [53].

2.4.3. BSA fluorescence quenching

Albumin proteins are known for their transportation and distribution of drugs to the bloodstream and thus their interactions with metal drugs may alter the biological properties of the drug [54]. We therefore studied the interactions of the palladium complexes **Pd1-Pd4** with bovine serum albumin protein in order to understand the binding modes and quenching mechanisms of these palladium complexes. Reductions in the fluorescence emission intensity at 348 nm upon the addition of increasing concentrations of **Pd1-Pd4** (Figs. 5, **S37–S39)** to a fixed concentration of bovine serum albumin were observed, indicating the change in the conformation of bovine serum albumin [55]. The Stern-Volmer (K_{sv}) and bimolecular constants (K_q) were determined from the Stern-Volmer equation ($(I_o/I = 1 + K_{sv}[Q] = 1 + k_q\tau_0[Q])$ and were used to describe the quenching mechanism of the complexes. The number of binding sites (n) and Scatchard constant (K_F) were determined from the Scatchard equation ($\log(I_o - I) / I = \log K_F + n \log[Q]$) and the linear plot as given in Fig. 5 and Table 2. The high magnitudes of the dynamic collision quenching constant K_{sv} (1.48–29.67) x 10^6 M^{-1} for compounds **Pd1-Pd4** were indicative of strong protein binding [56]. Furthermore, the bimolecular constants, k_q (0.66–13.99) x 10^{14} $M^{-1}s^{-1}$ are higher than the scattered collision quenching constant of 2.0×10^{10} $M^{-1}s^{-1}$ for biomolecules and thus supports the existence of a static quenching mechanism [26], consistent with the EB-CT-DNA results (Table 1). In addition, the higher values of K_{sv} and k_q indicate that the binding process is not entirely controlled by diffusion, but it appears some specific drug proteins also take part in the process, resulting in enhanced k_q constant [57]. These constants are comparable to the magnitude of (10^{14}) obtained for copper(II) and zinc(II) complexes of 4-acylpyrazolone ligands [58]. The computed K_F values (0.10–16.10) x 10^5 M^{-1} of complexes **Pd1-Pd4** (Table 2) are within the optimum range, required to promote strong binding of the complexes to the BSA and be transported to target DNA [59]. The number of binding sites n values (0.70–0.89) of **Pd1-Pd4** is closer to one, demonstrating that the compounds bind to a single site in BSA.

2.5. In vitro cytotoxicity of palladium complexes Pd1-Pd4

The cytotoxic activity of the four palladium(II) complexes **Pd1-Pd4** was examined in the human breast cancer cell lines MCF-7 (used for preliminary investigations) and MDA-MB-231, the transformed lung cell line MRC5-SV2 (a model of lung cancer), and the normal lung fibroblast cell line MRC5. Cisplatin, a platinum-based anticancer drug, was used as the positive control. The concentration range used for each tested compound was 6.25 – 100 μM, and treatment was for 48 h, after which the MTT assay was used to assess cell viability. As shown in Fig. 4**A**, cisplatin reduced cell viability in a concentration-dependent manner, with the effect of each tested concentration being significant. Complexes **Pd1-Pd4** also exhibited a concentration-dependent reduction in cell viability, although the MDA-MB-231 cell line was less sensitive to their cytotoxic effects compared to the MCF-7 and MRC5-SV2 cells (Fig. 4**B-D**). The IC_{50} values are shown in Table 3. Of the four palladium(II) complexes, **Pd1** was the most potent. It was potently cytotoxic against the MCF-7 cell line, with an IC_{50} value of 11.4 μM (although the effect was not clearly concentration-dependent), while **Pd4** was moderately cytotoxic against the cell line, with an IC_{50} value of 61.5 μM. **Pd1** also displayed significant cytotoxicity against the MRC5-SV2 cell line, with an IC_{50} value of 30.7 μM, whereas **Pd2** was inactive against it (IC_{50} value of 341.5 μM). The greater cytotoxic activity of complex **Pd1** in comparison to the complex **Pd4** could be associated with the dinuclear nature of complex **Pd1** relative to the mono-nuclear complex **Pd4**. Interestingly, complexes **Pd2** and **Pd3** were relatively inactive against the MCF-7 cell line, with IC_{50} values of 154.9 μM and 230.1 μM, respectively. In addition, all compounds were inactive against the MDA-MB-231 cell line, with IC_{50}>100 μM. Thus, the cytotoxic (potentially anticancer) activities of the palladium(II) complexes against the cancer cell lines studied generally follow the order **Pd1 > Pd4 > Pd2 > Pd3**.

In the design of chemotherapeutic drugs, one of the most desirable features is the development of a drug that kills cancer cells whilst sparing normal cells. Due to significant cytotoxicity against the MRC5-SV2 displayed by the **Pd1** cell line that is derived from the normal cell line MRC5 by transformation (IC_{50} =30.7 μM against MRC5-SV2) (Fig. 6 and Table 3), the effects **Pd1** against MRC5 were assessed. Significantly, complex **Pd1** exhibited lower toxicity against MRC5 than against MRC5-SV2, giving a selectivity index (SI) of 3.3. This SI value is better than that of cisplatin (IC_{50} =18.7 μM against MRC5) of 1.6 [42]. Therefore, in the drug discovery context, compound **Pd1** is promising in its current form for potential applications in chemotherapy. Similarly, complex **Pd1** (IC_{50} =177.6 μM**)**, showed comparable potency against the MDA-MB-231 cell line to cisplatin (IC_{50} >200 μM)[60]within 24 h of exposure (Table 3). However, complex the IC_{50} of 11.2 μM reported for complex is **Pd1** against the MCF-7 cell line much lower compared to the value of 0.65 μM previously reported by Saa and co-workers [61].

Further attempts were made to correlate the relative cytotoxicity of the palladium complexes with their respective DNA & BSA binding affinities to establish any dependency or trend. From the summarised data shown in Table 3, the palladium(II) complex **Pd2** showed the highest BSA binding interactions ($K_F = 16.10 \pm 0.82 \times 10^5$ M^{-1}), while complex **Pd3** displayed the highest DNA binding constants ($K_F = 53.44 \pm 2.74 \times$

Table 1
CT-DNA binding constants, quenching constants, and Gibbs energy values for **Pd1-Pd4**.

Complex	UV titration	EB fluorescence exchange titration					
	K_b x 10^6 (M^{-1})	K_{sv} x 10^5 (M^{-1})	K_{app} x 10^6 (M^{-1})	k_q x 10^{12} (M^{-1} s^{-1})	K_F x 10^4 (M^{-1})	n	$\Delta G_{25\,^\circ C}$/kJmol^{-1}
Pd1	4.78 ± 0.27	9.71 ± 0.48	8.07 ± 0.34	2.61 ± 0.61	1.11 ± 0.170	0.84	−38.1
Pd2	10.80 ± 0.98	23.14 ± 1.56	14.52 ± 1.41	1.02 ± 1.12	1.42 ± 0.14	0.75	−401.3
Pd3	13.12 ± 0.91	28.41 ± 2.43	25.02 ± 2.74	12.33 ± 1.91	53.44 ± 2.74	1.08	−406.1
Pd4	4.28 ± 0.41	1.82 ± 0.14	3.93 ± 0.11	1.00 ± 0.02	1.01 ± 0.17	0.94	−36.0

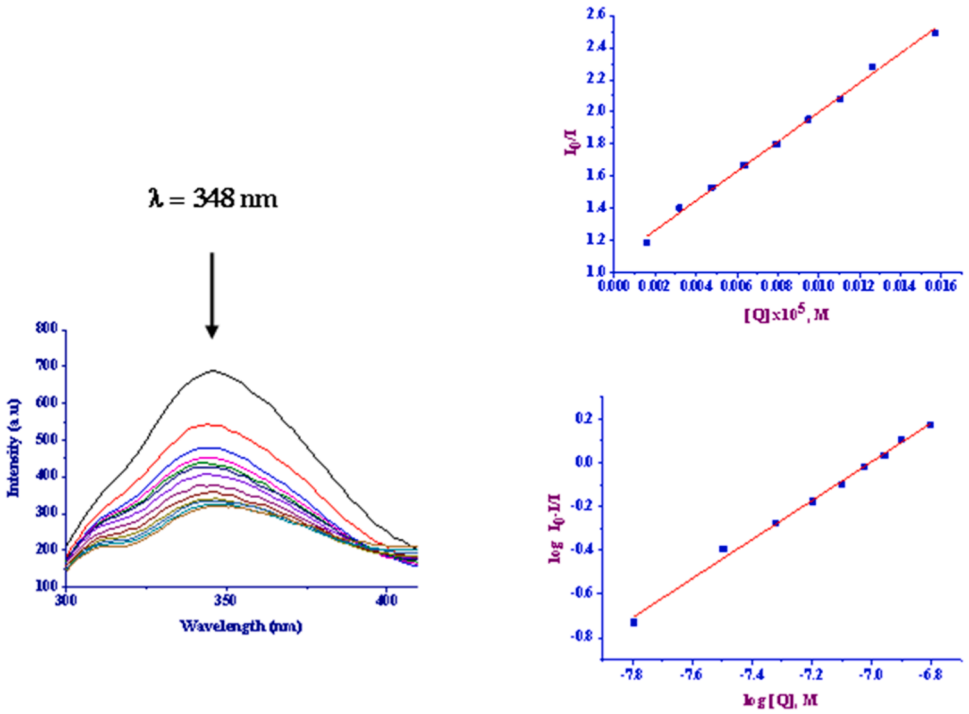

Fig. 5. Quenching in fluorescence emission spectra of BSA in the presence of increasing concentrations of **Pd3** = 0–40 μM and [BSA] = 14 μM. The arrow shows the decrease in fluorescence intensity upon increasing the **Pd3** concentration. Inserted is the Stern-Volmer plot of I_o/I vs [Q] and Scatchard plot of log[(I_o–I)/I] vs log[Q].

Table 2
BSA binding constants, quenching constants, and number of binding sites for **Pd1-Pd4**.

Complex	K_{sv} x 10^6 (M^{-1})	k_q x 10^{14} (M^{-1} s^{-1})	K_F x 10^5 (M^{-1})	*n*
Pd1	9.18 ± 0.76	4.14 ± 0.21	8.43 ± 0.23	0.89
Pd2	29.67 ± 2.87	13.99 ± 0.97	16.10 ± 0.82	0.71
Pd3	7.95 ± 0.89	3.55 ± 0.18	0.15 ± 0.01	0.80
Pd4	1.48 ± 0.15	0.66 ± 0.05	0.10 ± 0.01	0.70

Table 3
IC_{50} values of palladium(II) complexes (**Pd1-Pd4**) against MCF-7 and MDA-MB-231 cancer cell lines, and the transformed human lung cell line MRC5-SV2, and DNA/BSA binding constants.

Compound	IC_{50} (μM)			Binding constants	
	MCF-7	MDA-MB-231	MRC5-SV2	DNA/K_F x10^4 (M^{-1})	BSA/K_F x10^5 (M^{-1})
Pd1	11.2	177.6	30.7	1.11 ± 0.17	8.43 ± 0.23
Pd2	154.9	268.1	298.1	1.42 ± 0.14	16.10 ± 0.82
Pd3	230.1	209.7	116.8	53.44 ± 2.74	0.15 ± 0.01
Pd4	61.5	150.9	341.5	1.01 ± 0.17	0.10 ± 0.01
Cisplatin	0.65 [61]	>200[60]	11.4[42]		

10^4 M^{-1}). Interestingly, **Pd2** and **Pd3** were inactive against the MCF-7 cell line, whereas all compounds were inact[60]ive against the MDA-MB-231 cell line, with IC_{50} values >100 μM, and **Pd2-Pd4** were inactive against MRC5-SV2, with IC_{50} values >200 μM, respectively. **Pd1** and **Pd4** with lower DNA interactions (1.11 ± 0.17 × 10^4 M^{-1} and 1.01 ± 0.17 × 10^4 M^{-1}, respectively) were active against the MCF-7 cell line, displaying IC_{50} values of 11.2 μM and 61.5 μM, respectively (Table 3). One would thus expect complexes **Pd2** and **Pd3** to display higher cytotoxicity in comparison to complexes **Pd1** and **Pd4** [62]. The opposite results observed in this study thus highlight that the cytotoxicity of these complexes is not entirely dependent on the respective DNA/BSA interactions, but could also be a result of other factors such as solubility, permeability, and lability [22].

3. Conclusions

(Pyridyl)pyrazine carboxamide-based ligands (**L1**-**L4**) form dinuclear and mononuclear palladium complexes, depending on the nature and denticity of the ligand. While bidentate ligands (**L1**-**L3**) formed dinuclear complexes, the tridentate ligand **L4** forms mononuclear complexes. All the complexes showed favorable CT-DNA and BSA binding interactions via intercalating mode and static mechanism, respectively. In general, dinuclear complexes **Pd1-Pd3** showed stronger DNA interactions than the mononuclear complex **Pd4.** The palladium(II) complexes (**Pd1**-**Pd4**) were investigated for their cytotoxic activity against the MCF-7 and MDA-MB-231 cancer cell lines and the transformed MRC5-SV2 cancer cell line. **Pd2** and **Pd3** were generally inactive, while **Pd1** and **Pd4** displayed high and moderate cytotoxic activities, respectively, against MCF-7. All the compounds were inactive against MDA-MB-231, while complexes **Pd2-Pd4** were inactive against MRC5-SV2. Significantly, when one of the compounds that were active against MCF-7 (**Pd1**) was assessed for selectivity by testing it against both the transformed cell line MRC5-SV2 and its parental normal cell line MRC5, it exhibited relatively low toxicity against MRC5 (i.e., high selectivity index). Thus, the introduction of alkyl substituents on the aryl ring lowers the cytotoxicity of the palladium complexes. In addition, both the coordination chemistry of the compounds and the nature of the cancer cell lines significantly determined their cytotoxicity. There was no clear correlation between the cytotoxicity and DNA/BSA interactions of the complexes, pointing to complex mechanisms underpinning their cytotoxic action and potentially their anti-cancer activities.

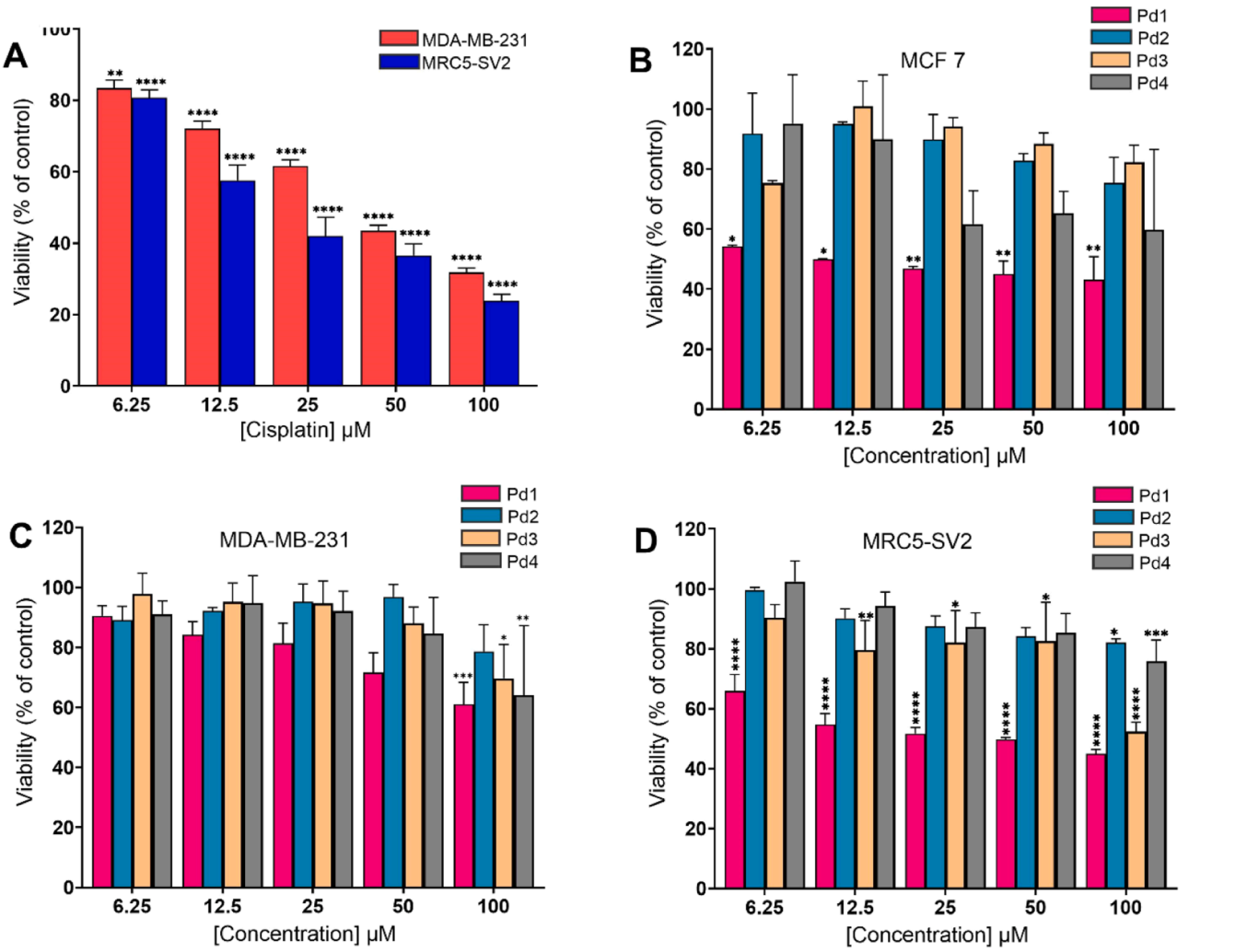

Fig. 6. Effects of cisplatin (positive control) and the palladium (II) complexes **Pd1-Pd4** on the viability of the cancer cell lines MCF-7 and MDA-MB-231, and the transformed cell line MRC5-SV2, after 48 h treatment. Each bar represents the Mean ± SEM of percentage cell viability ($n = 2$ for MCF-7 and $n = 3$–4 for MBA-MB-231 or MRC5-SV2). *$P < 0.05$, **$P < 0.01$, ***$P < 0.001$ and ****$P < 0.0001$ compared to the negative control.

4. Experimental section

4.1. General materials and instrumentation

Air- and water-sensitive compounds were synthesized under a nitrogen atmosphere using the standard Schlenk techniques. The solvent diethyl ether was dried over distillation using calcium hydride and dichloromethane was purified by distillation using P_2O_5. The solvents were stored in molecular sieves, respectively. Acetonitrile, chloroform, and ethanol obtained from Merck were of analytical grade. Chemical reagents, including pyrazine-2,3-dicarboxylic acid (>97 %), 2-amino-4-methylpyridine (>99 %), 2-amino-6-methylpyridine (>98 %), 2-aminopyridine (>99 %), triphenylphosphite (>97 %), and 8-aminoquinoline (>98 %) were purchased from Merck and used without further purification. The starting material, $[PdCl_2(NCMe)_2]$, was prefabricated by adopting a literature procedure [63].

^1H and $^{13}C\{^1H\}$ NMR spectra were recorded on a Bruker 400 MHz spectrometer in DMSO-d_6 at room temperature, and chemical shifts were reported in ppm with reference to tetramethyl silane $(CH_3)_4Si$. FT-IR spectra of all ligands and complexes were determined on Bruker Apex 2.0 using OPUS programme in 4000–500 cm^{-1} range. Mass spectral analyses were acquired on a Shimadzu LC-MS Spectrometer and Waters LCT Premier Spectrometer TOF micro-mass. Elemental analyses were carried out on Thermal Scientific Flash 2000. Calf-thymus DNA, ethidium bromide, and bovine serum albumin were purchased from Merck and used without any further purification. Ultrapure water was used in the experiments. CT-DNA titrations were performed on a Cary 100 Series UV–vis spectrophotometer with a temperature controller (± 0.05 °C). Fluorescence quenching experiments were performed on a Perkin Elmer LS 45 Fluorescence Spectrometer using 1 cm path length cuvettes at room temperature.

4.2. Single crystal X-ray crystallography analyses

Single crystal X-ray crystallography analyses of compounds **Pd1** and **Pd3** were measured on Bruker Apex Duo diffractometer made up of an Oxford Instruments Cryojet operating at 100(22) K and a Incoatec microsource operating at 30 W. Data for the molecular structures **Pd1** and **Pd3** were obtained by recording the measurements under the following conditions: Mo Kα (λ= 0.71073 Å) radiation at crystal-to-detector distance of 50 mm at omega and phi scans with exposures taken at 30 W-X-ray power and 0.50° frame widths using APEX-II conditions. Using SHELX-2014 [64] and OLEX2 [65] direct methods, the molecular structures of **Pd1** and **Pd3** were solved and further refined with SHELX-2014 least squares approach [66]. All hydrogen atoms were incorporated as idealised contributors. In addition, standard riding model was utilised in calculating the position of all hydrogen, with C—$H_{aromatic}$ distances of 0.93 Å and U_{iso}= 1.2U_{eq}, C—$H_{methylene}$

distances of 0.99 Å and U_{iso}= 1.2U_{eq} and C—H_{methyl} distances of 0.98 Å and U_{iso}= 1.5U_{eq}. All non-hydrogen atoms were refined anisotropically with SHELX-2014.

4.3. Syntheses of (pyridyl)pyrazine carboxamide palladium(II) complexes

4.3.1. $[Pd_2(L1)_2Cl_2]$ (Pd1)

A solution of N^2, N^3-bis(4-methylpyridin-2-yl)pyrazine-2,3-dicarboxamide (**L1**) (0.12 g, 0.17 mmol) in acetonitrile was added to a stirring solution of $[PdCl_2(NCMe)_2]$ (0.10 g, 0.37 mmol) in acetonitrile. The mixture was refluxed under nitrogen for 24 h, resulting in a yellow precipitate. The precipitate was filtered and washed with chloroform, followed by diethyl ether to give a yellow solid. Yield: 0.20 g (57 %).^{1}H NMR (400 MHz, DMSO-d_6): δ_H(ppm): 7.02(m, 2H, $H_{pyrdine}$); 7.72(m, 2H, $H_{pyridine}$); 7.44 (d, $^3J_{HH}$ = 8.1, 2H, $H_{pyridine}$); 7.75 (m, 2H, $H_{pyridine}$); 7.88 (m, 2H, $H_{pyridine}$); 8.22 (d, $^3J_{HH}$ = 8.5, 2H, $H_{pyridine}$); 8.37 (m, 2H, $H_{pyridine}$); 8.44 (m, 2H, $H_{pyridine}$); 9.12 (m, 4H, $H_{pyrazine}$); 11.09 (s, H, NH_{amide}). ^{13}C{^{1}H} NMR (100MHz, DMSO-d_6): 114.5 ($C_{aromatic}$); 120.8 ($C_{aromatic}$); 139.4 ($C_{aromatic}$); 145.9 $C_{aromatic}$); 148.4 ($C_{aromatic}$); 148.6 ($C_{aromatic}$); 151.4 ($C_{aromatic}$); 160.1 ($C_{carbornyl}$); 163.7 ($C_{carbonyl}$). FT-IR spec (cm^{-1}): υ(N—H) = 3271, υ(C = O) =1705, 1642. (TOF-MS): *m/z*, for $C_{32}H_{22}Cl_2N_{12}O_4Pd_2$ = 922.96 [M^+]. Anal. Cald. $C_{32}H_{22}N_{12}O_4Cl_2Pd_2$: C, 41.67; H, 2.40; N, 18.22. Found (%): C, 41.54; H, 2.76; N, 18.20.

Complexes **Pd2** and **Pd3** were synthesized following a similar procedure to the one described for **Pd1**.

4.3.2. $[Pd_2(L2)_2Cl_2]$ (Pd2)

N^2, N^3-bis(4-methylpyridin-2-yl)pyrazine-2,3-dicarboxamide (**L2**) (0.13 g, 0.37 mmol) and $[PdCl_2(NCMe)_2]$ (0.10 g, 0.37 mmol). A yellow solid was obtained. Yield: 0.14 g (37 %). ^{1}H NMR (400 MHz, DMSO-d_6): δ_H(ppm): 2.43(s, 3H, H_{methyl}); 2.99(s, 3H, H_{methyl}); 6.98 (d, $^3J_{HH}$ = 7.5, 2H, $H_{pyridine}$); 7.06 (d, $^3J_{HH}$ = 7.6 2H, $H_{pyridine}$); 7.30 (d, $^3J_{HH}$ = 7.9, 2H, $H_{pyridine}$); 7.66–7.70 (t, $^3J_{HH}$ =7.8, 2H, $H_{pyridine}$); 7.73–7.77 (t, $^3J_{HH}$ = 7.9, 2H, $H_{pyridine}$); 8.04 (d, $^3J_{HH}$ =8.2, 2H, $H_{pyridine}$); 9.07 (s, 4H, $H_{pyrazine}$);10.97 (s, 2H, NH_{amide}). ^{13}C{^{1}H} NMR (100 MHz, DMSO-d_6): 23.9 (C_{methyl}); 25.5 (C_{methyl}); 111.3 ($C_{aromatic}$); 119.6 ($C_{aromatic}$); 119.9 ($C_{aromatic}$); 139.2 ($C_{aromatic}$); 139.5 ($C_{aromatic}$);145.8 ($C_{aromatic}$); 150.8 ($C_{aromatic}$); 151.4 $C_{aromatic}$); 157.1 ($C_{aromatic}$); 157.3 ($C_{aromatic}$); 159.3 ($C_{aromatic}$); 163.2 ($C_{carbornyl}$); 166.9 ($C_{carbonyl}$) FT-IR spec (cm^{-1}): υ (N—H) = 3444 υ(C = O) $_{amide}$ =1635. (TOF-MS): *m/z*, $C_{36}H_{30}Cl_2N_{12}O_4Pd_2$. = 1000.2 [$M^+$ + Na]. Anal. Cald. $C_{36}H_{30}N_{12}O_4Cl_2Pd_2$: C, 44.19; H, 3.09; N, 17.18. Found (%): C, 44.53; H, 2.97; N, 17.35.

4.3.3. $[Pd_2(L3)_2Cl_2]$ (Pd3)

N^2,N^3-bis(4-methylpyridin-2-yl)pyrazine-2,3-dicarboxamide (**L3**) (0.13 g, 0.37 mmol) and $[PdCl_2(NCMe)_2]$ (0.10 g, 0.37 mmol) and refluxed for 24 h. A yellow solid was isolated. Yield: 0.11 g (30 %). ^{1}H NMR (400 MHz, DMSO-d_6): δ_H(ppm): 2.27(s, 3H, H_{methyl}); 2.38(s, 3H, H_{methyl}); 6.88 (m, H, $H_{pyridine}$); 7.04(m, H, $H_{pyridine}$); 7.27(s, H, $H_{pyridine}$); 8.08(s, H, $H_{pyridine}$); 8.22–8.26 (m, 2H, $H_{pyridine}$); 9.09–9.12 (m, 4H, $H_{pyrazine}$); 11.02 (s, 2H, NH_{amide}). ^{13}C{^{1}H} NMR (100 MHz, DMSO-d_6): 20.6 (C_{methyl}); 21.3 (C_{methyl}); 114.8 ($C_{aromatic}$); 122.8 ($C_{aromatic}$); 124.6 ($C_{aromatic}$); 144.0 ($C_{aromatic}$);149.5 ($C_{aromatic}$); 150.2 ($C_{aromatic}$); 151.8 $C_{aromatic}$); 152.3($C_{aromatic}$); 153.1 ($C_{aromatic}$); 159.3 ($C_{aromatic}$); 163.4 ($C_{carbornyl}$); 166.9 ($C_{carbonyl}$) FT-IR spec (cm^{-1}): υ(N—H) = 3495, υ(C = O)$_{amide}$ =1705, υ(O = C—N)= 1632. (TOF-MS): *m/z*, $C_{36}H_{30}Cl_2N_{12}O_4Pd_2$ = 979.10 [M^+ + *H*]. Anal. Cald. $C_{36}H_{30}N_{12}O_4Cl_2Pd_2$: C, 44.19; H, 3.09; N, 17.18. Found (%): C, 44.32; H, 2.89; N, 17.36.

4.3.4. [Pd(L4)Cl] (Pd4)

To a stirring solution of $[PdCl_2(NCMe)_2]$ (0.11 g, 0.39 mmol) in CH_2Cl_2 (10 ml) a solution of *N^2, N^3-bis(quinoline-8-yl)pyrazine-2,3-dicarboxamide* (**L4**) (0.16 g, 0.39 mmol) in CH_2Cl_2 (10 ml) was slowly added and the mixture was stirred for 12 h at room temperature. Dark red solid was obtained, filtered, and washed thoroughly with dichloromethane. Yield: 0.11 g, (85 %). ^{1}H NMR (400 MHz, DMSO-d_6): δ_H(ppm): 7.59 (m, H, $H_{quinoline}$) 7.66 (m, H, $H_{quinoline}$) 7.70(m, H, H $_{quinoline}$) 7.75 (t, $^3J_{HH}$ = 8.0, H, $H_{quinoline}$), 7.77 (m, H, $H_{quinoline}$), 7.81 (m, H, $H_{quinoline}$), 8.47 (, H, $H_{quinoline}$), 8.54 (d, $^3J_{HH}$ = 7.7, H, $H_{quinoline}$) 8.72 (d, $^3J_{HH}$ = 8.5, H, $H_{quinoline}$), 8.85 (m, H, $H_{quinoline}$), 8.87 (m, H, $H_{quinoline}$), 8.89 (m, 3H, $H_{quinoline}$); 8.91 (m, H, $H_{pyrazine}$), 9.08 (d, $^3J_{HH}$ = 2.8 H, $H_{pyrazine}$), 11.02 (s, 2H, NH_{amide}). ^{13}C{^{1}H} NMR (100 MHz, DMSO-d_6): 118.1 ($C_{aromatic}$); 120.5 ($C_{aromatic}$); 122.4 ($C_{aromatic}$); 122.5 ($C_{aromatic}$); 123.1 ($C_{aromatic}$); 123.2 ($C_{aromatic}$); 127.8 ($C_{aromatic}$);128.4 ($C_{aromatic}$); 129.8 ($C_{aromatic}$); 130.7 $C_{aromatic}$); 135.2($C_{aromatic}$); 137.1 ($C_{aromatic}$); 138.8 ($C_{aromatic}$); 140.9 ($C_{aromatic}$); 143.3 ($C_{aromatic}$); 144.5 ($C_{aromatic}$); 147.4 ($C_{aromatic}$); 147.8 ($C_{aromatic}$); 149.3 ($C_{aromatic}$);149.5 ($C_{aromatic}$); 151.5 ($C_{aromatic}$); 153.1 ($C_{aromatic}$); 163.3 ($C_{carbornyl}$); 165.4 ($C_{carbonyl}$). FT-IR spec (cm^{-1}): υ(N—H) = 3390, υ(C=O)$_{amide}$ = 1686, 1636. HR-MS: *m/z*, Calc for $C_{18}H_{11}N_6O_2ClPd$ = 560.14 Found: 561.0045 [M^+ +H]. Anal. Calc. (%) for $C_{18}H_{11}N_6O_2ClPd$: C, 44.56; H, 2.29; N, 17.32. Found (%): C, 44.25; H, 2.13; N, 17.25.

4.5. Stability of the complexes in aqueous and DMSO solutions

The solution stability of the complexes **Pd1** and **Pd4** in aqueous, PBS (pH = 7.4) or DMSO media were investigated using ^{1}H NMR and UV-visible spectroscopies. The solutions were prepared and scanned promptly, and the UV-visible spectral data were recorded over a period of 48 h at room temperature.

4.6. In vitro cytotoxicity

Two human breast cancer cell lines (MCF-7 and MDA-MB-231), a transformed human foetal lung cell line (MRC5-SV2, a model of lung cancer), as well as a normal human foetal lung fibroblast cell line (MRC-5) were used to examine the cytotoxic effects of the palladium(II) complexes (**Pd1**-**Pd4**) using methods as we previously reported [42,67]. In brief, the cells were grown as adherent monolayer cultures in 75cm^2 tissue culture flasks (T75) using Dulbecco's Modified Eagle Medium (DMEM) supplemented with 10 % Foetal Calf Serum, 2 mM L-glutamine, and 1 % antibiotic-antimycotic solution (containing penicillin, streptomycin, and amphotericin B), and incubated at 37 °C in a humidified atmosphere of 5 % CO_2. Upon reaching about 80 % confluency, a flask of cells was decanted (medium removed), rinsed with phosphate-buffered saline (PBS), and trypsinised for 1 min. Trypsin (TrypLE) was removed, the flask was incubated for 3–5 min, and then flooded with growth medium. A suspension of single cells was made by trituration, and the density of the suspension was determined using a haemocytometer (counting aided by a microscope). The density was diluted to 5 × 10^4 cells/ml, and 100 μL of the diluted suspension was added to each well of a micro-clear, flat-bottom 96-well plate, which was then incubated for 24 h. Cells were then treated (in triplicate) for 48 h. To assess cell viability following treatment, the MTT assay was carried out (10 % MTT solution (5 mg/ml) added to each well for 4 h, well content removed, DMSO added to solubilise formazan crystals, plate gently shaken on an orbital shaker, and absorbance of plate read at 570 nm using the Tecan Spark 10 M microplate reader), as previously reported [38]. The viability of each treatment was expressed as a percentage of the negative (vehicle) control. Data is presented as Mean ± SEM (Standard Error of the Mean) for the indicated number of independent experiments. Data analysis and statistical analysis were done using GraphPad Prism version 10.2.3 for Windows, GraphPad Software, Boston, Massachusetts, USA, www.graphpad.com. Statistical significance of differences between three or more means was assessed using One-way Analysis of Variance (ANOVA) followed by Tukey's post hoc test for multiple comparisons. A *P*-value of <0.05 was considered statistically significant. IC_{50} was determined by fitting the data to the non-linear regression "log [inhibitor] versus response (three parameters)", while Selectivity Index was

calculated by dividing the IC_{50} of the normal cell line by the IC_{50} of the cancer (or transformed) cell line.

CRediT authorship contribution statement

Sabathile T. Mvelase: Writing – original draft, Methodology, Investigation, Formal analysis. **Saheed O. Benson:** Validation, Software, Methodology, Formal analysis, Data curation. **Reinner O. Omondi:** Writing – original draft, Visualization, Data curation, Conceptualization. **Robert T. Kumah:** Writing – original draft, Methodology, Formal analysis, Conceptualization. **Amos A. Fatokun:** Writing – review & editing, Resources, Project administration, Investigation, Funding acquisition. **Stephen O. Ojwach:** Writing – review & editing, Supervision, Resources, Project administration, Funding acquisition, Conceptualization.

Declaration of competing interest

The authors have no known conflicts of interests to declare.

Data availability

Data available as electronic supplementary materials.

Acknowledgments

We acknowledge the financial assistance the National Research Foundation (NRF). We are also grateful to Dr Leigh Hunter for assistance with single crystal X-ray data collection and refinement of complexes **Pd1** and **Pd3**.

Supplementary materials

Supplemental material contains analytical data (NMR and FT-IR spectroscopic spectral data, mass spectral, and single X-ray crystallography data and files). The material also contains DNA binding UV-visible and fluorescence spectra and BSA fluorescence spectra. The crystallographic data entry for compounds **Pd1** and **Pd3** are given by the deposition numbers CCDC 2,361,599 and 236,601 respectively.

Supplementary material associated with this article can be found, in the online version, at doi:10.1016/j.molstruc.2024.140267.

References

[1] G. Ayyannan, M. Mohanraj, M. Gopiraman, R. Uthayamalar, G. Raja, N. Bhuvanesh, R. Nandhakumar, C. Jayabalakrishnan, New Palladium (II) complexes with ONO chelated hydrazone ligand: Synthesis, characterization, DNA/BSA interaction, antioxidant and cytotoxicity, Inorg. Chim. Acta. 512 (2020) 119868.

[2] D.P. Dorairaj, J. Haribabu, Y.L. Chang, C. Echeverria, S.C. Hsu, R. Karvembu, Pd (II)–PPh_3 complexes of halogen substituted acylthiourea ligands: Biomolecular interactions and in vitro anti-proliferative activity, Appl, Organomet. Chem. 36 (8) (2022) e6765.

[3] K. Karami, N. Jamshidian, M. Zakariazadeh, N-palladacycles containing pyridinium-derived ligands: DNA and BSA interaction studies and evaluation as anti-tumor agents, Appl, Organomet. Chem. 33 (3) (2019) e4728.

[4] M. Aminzadeh, H. Mansouri-Torshizi, R. Aleeshah, K. Abdi, M. Saeidifar, A new palladium-based antiproliferative agent: synthesis, characterization, computational calculations, cytotoxicity, and DNA binding, properties, Biometals 34 (5) (2021) 1173–1189.

[5] R. Bhaduri, A. Pan, S.K. Tarai, S. Mandal, A. Bagchi, A. Biswas, S.C. Moi, In vitro anticancer activity of Pd (II) complexes with pyridine scaffold: Their bioactivity, role in cell cycle arrest, and computational study, J. Mol. Liq. 367 (2022) 120540.

[6] A.S Dorafshan Tabatabai, E. Dehghanian, H. Mansouri-Torshizi, Probing the interaction of new and biologically active Pd (II) complex with DNA/BSA via joint experimental and computational studies along with thermodynamic, NLO, FMO and NBO analysis, Biometals 35 (2) (2022) 245–266.

[7] R. Naskar, P. Ghosh, S. Mandal, S. Jana, N. Murmu, T.K. Mondal, Palladium (II) complex bearing benzothiazole based O, N, S donor pincer ligand: Study of in-vitro cytotoxicity, interaction with CT-DNA and BSA protein, J. Chem. Sci. 134 (4) (2022) 103.

[8] E.Z. Jahromi, A. Divsalar, A.A. Saboury, S. Khaleghizadeh, H. Mansouri-Torshizi, I. Kostova, Palladium complexes: new candidates for anti-cancer drugs, J. Iran. Chem. Soc. 13 (2016) 967–989.

[9] S. Rajković, A.A. Franich, V. Ćupurdija, M.D. Živković, DNA-and BSA-Binding Studies of Dinuclear Palladium (II) Complexes with 1, 5-Naphtiridine Bridging Ligands, EABR (2021), https://doi.org/10.2478/sjecr-2021-0030.

[10] M. Glišić, P.P. Čanović, M.M. Zarić, R.S. Živković Zarić, A. Franich, S. Rajković, M. Živković, The cytotoxicity of palladium (II) complexes containing 1, 2-or 1, 4-diazine bridging ligands on squamous cell carcinoma cells in vitro: Insights in the mechanisms of action, Appl. Organomet. Chem. (2024) e7449.

[11] Z. Wang, J. Li, R. Liu, X. Jia, H. Liu, T. Xie, H. Chen, L. Pan, Z. Ma, Synthesis, characterization and anticancer properties: A series of highly selective palladium (II) substituted-terpyridine complexes, J. Inorg. Biochem. 244 (2023) 112219.

[12] C. Panda, A. Sarkar, S.S. Gupta, Coordination chemistry of carboxamide 'Nx'ligands to metal ions for bio-inspired catalysis, Coord. Chem. Rev. 417 (2020) 213314.

[13] B.P.R. Aradhyula, W. Kaminsky, M.R. Kollipara, Half-sandwich d^6 metal complexes with bis (pyridine carboxamide) benzene ligand: Synthesis and spectral analysis, J. Mol. Struct. 1149 (2017) 162–170.

[14] W. Jacob, R. Mukherjee, Synthesis, structure, and properties of monomeric Fe (II), Co (II), and Ni (II) complexes of neutral N-(aryl)-2-pyridinecarboxamides, Inorg. Chim. Acta. 359 (14) (2006) 4565–4573.

[15] A. Rajput, R. Mukherjee, Coordination chemistry with pyridine/pyrazine amide ligands. Some noteworthy results, Coord, Chem. Rev. 257 (2) (2013) 350–368.

[16] S.H. van Rijt, A.J. Hebden, T. Amaresekera, R.J. Deeth, G.J. Clarkson, S. Parsons, P. C. McGowan, P. Sadler, Amide linkage isomerism as an activity switch for organometallic osmium and ruthenium anticancer complexes, J. Med. Chem. 52 (23) (2009) 7753–7764.

[17] M. Juribašić, K. Molčanov, B. Kojić-Prodić, L. Bellotto, M. Kralj, F. Zani, L. Tušek-Božić, Palladium (II) complexes of quinolinylaminophosphonates: Synthesis, structural characterization, antitumor and antimicrobial activity, J. Inorg. Biochem. 105 (6) (2011) 867–879.

[18] S.R. Majeed, M.A. Amin, F.A. Attaby, A.A. Soliman, Palladium Complexes Based on 2-Hydrazinopyridine Ligand: Synthesis, Spectroscopic Studies, DFT Calculations, and Cytotoxicity, Biointerface Res. App. Chem. 11 (2021) 14316–14335.

[19] G. Zhao, H.J.C.M. Lin, Metal complexes with aromatic N-containing ligands as potential agents in cancer treatment, Curr, Med. Chem. Anticancer Agents 5 (2) (2005) 137–147.

[20] M.N. Zafar, A.M. Butt, F. Perveen, M.F. Nazar, S. Masood, A.F. Dalebrook, E. U. Mughal, S.H. Sumrra, Y.Y. Sung, T.S.T. Muhammad, Pd(II) complexes with chelating N-(1-alkylpyridin-4 (1H)-ylidene) amide (PYA) ligands: Synthesis, characterization and evaluation of anticancer activity, J. Inorg. Biochem. 224 (2021) 111590.

[21] S.G. Churusova, D.V. Aleksanyan, A.A. Vasil'ev, E.Y. Rybalkina, O.Y. Susova, Z. S. Klemenkova, R.R. Aysin, Y.V. Nelyubina, V.A. Kozlov, Design of pincer complexes based on (methylsulfanyl) acetic/propionic acid amides with ancillary S-and N-donors as potential catalysts and cytotoxic agents, Appl. Organomet. Chem. 32 (6) (2018) e4360.

[22] R.O. Omondi, S.O. Ojwach, D. Jaganyi, Review of comparative studies of cytotoxic activities of Pt (II), Pd (II), Ru (II)/(III) and Au (III) complexes, their kinetics of ligand substitution reactions and DNA/BSA interactions, Inorg. Chim. Acta 512 (2020) 119883.

[23] T.J. Carneiro, A.S. Martins, M.P.M. Marques, A.M. Gil, Metabolic aspects of palladium (II) potential anti-cancer drugs, Front. Oncol 10 (2020) 590970.

[24] N. Alisufi, H. Mansouri-Torshizi, Preparation, characterization, DNA/BSA interaction and computational binding analyses of a dinuclear, biopotency Pd+ 2 coordinated with 1, 4-phenylenediamine and ethylenediamine as ligands, J. Iran. Chem. Soc. 18 (5) (2021) 1147–1166.

[25] F. Mohammadlou, H. Mansouri-Torshizi, K. Abdi, Dynamics, Interaction of bis (alkylamine) dichloropalladium (II) complexes with CT-DNA and BSA; their synthesis, characterization, antitumor, and antibacterial evaluations, J. Biomol. Struct. Dyn. 39 (4) (2021) 1354–1372.

[26] R.O. Omondi, N.R. Sibuyi, A.O. Fadaka, M. Meyer, D. Jaganyi, S.O. Ojwach, Role of π-conjugation on the coordination behaviour, substitution kinetics, DNA/BSA interactions, and in vitro cytotoxicity of carboxamide palladium (II) complexes, Dalton, Trans. 50 (23) (2021) 8127–8143.

[27] E.J. Barreiro, A.E. Kümmerle, C.A. Fraga, The methylation effect in medicinal, chemistry, Chem. Rev. 111 (9) (2011) 5215–5246.

[28] V.N. Shinde, N. Bhuvanesh, A. Kumar, H. Joshi, Design and syntheses of palladium complexes of NNN/CNN pincer ligands: catalyst for cross dehydrogenative coupling reaction, of heteroarenes, Organometallics 39 (2) (2020) 324–333.

[29] R.T. Kumah, P. Vijayan, S.O. Ojwach, Carboxamide carbonyl-ruthenium (ii) complexes: Detailed structural and mechanistic studies in the transfer hydrogenation of ketones, New J. Chem. 46 (7) (2022) 3146–3155.

[30] M. Kiani, M. Bagherzadeh, S. Meghdadi, F. Fadaei-Tirani, K. Schenk-Joß, N. Rabiee, Catalytic and antibacterial properties of 3-dentate carboxamide Pd/Pt complexes obtained via a benign route, Appl. Organomet. Chem. 34 (4) (2020) e5531.

[31] S. Meghdadi, M. Amirnasr, A. Amiri, Z.M. Mobarakeh, Z. Azarkamanzad, Benign synthesis of N-(8-quinolyl) pyridine-2-carboxamide) ligand (Hbpq), and its Ni (II) and Cu (II) complexes. A fluorescent probe for direct detection of nitric oxide in acetonitrile solution based on Hbpq copper (II) acetate interaction, C.R Chim. 17 (5) (2014) 477–483.

[32] S. Meghdadi, V. Langer, H. Farrokhpour, A.A. Massoud, M. Amirnasr, Synthesis, X-ray structure, electrochemistry, and theoretical studies of palladium (II) complex with a tetradentate bis (quinoline-2-carboxamide) ligand, J. Iran. Chem. Soc. 9 (2012) 85–92.

[33] A.V. Kletskov, N.A. Bumagin, S.K. Petkevich, E.A. Dikusar, A.S. Lyakhov, L. S. Ivashkevich, I.A. Kolesnik, V.I. Potkin, Mimics of pincer ligands: an accessible Phosphine-Free N-(Pyrimidin-2-yl)-1, 2-azole-3-Carboxamide framework for Binuclear Pd (II) complexes and high-turnover catalysis in water, Inorg. Chim. Acta 59 (15) (2020) 10384–10388.
[34] S. Li, H. Wen, N. Yuan, P. Xie, J. Qin, Z. Wang, Synthesis, characterization and computational studies of Zn complex based on the 8-hydroxyquinoline group containing benzimidazole, RSC Adv. 10 (54) (2020) 32490–32496.
[35] S. Meghdadi, M. Amirnasr, M. Kiani, F Fadaei Tirani, M. Bagheri, K. Schenk, Benign synthesis of quinolinecarboxamide ligands, H2bqbenzo and H2bqb and their Pd(II) complexes: X-ray crystal structure, electrochemical and antibacterial studies, Coord Chem. 70 (14) (2017) 2409–2424.
[36] M. Sudharsan, M. Nethaji, N.S. Bhuvanesh, D. Suresh, Heteroleptic Palladium (II) Complexes of Thiazolinyl-picolinamide Derived N∩ N∩ N Pincer Ligand: An Efficient Catalyst for Acylative Suzuki Coupling Reactions, Asian. J. Org. Chem. 10 (11) (2021) 2982–2992.
[37] F.H. Allen, The Cambridge Structural Database: a quarter of a million crystal structures and rising, Acta Crystallogr. B: Struct. Sci. 58 (3) (2002) 380–388.
[38] C.R. Groom, I.J. Bruno, M.P. Lightfoot, S.C. Ward, The Cambridge structural database, Acta Crystallogr. B: Struct. Scie. Cryst. Eng. Mater. 72 (2) (2016) 171–179.
[39] S.R.I. Cooper, Showcasing research from Andre Frade and Richard Cooper from the Chemical Crystallography lab at the University of Oxford and Patrick McCabe at the Cambridge Crystallographic Data Centre, Cryst. Eng. Comm. 22 (2020) 7186.
[40] S. Sakaguchi, K.S. Yoo, J. O'Neill, J.H. Lee, T. Stewart, K.W. Jung, Chiral Palladium (II) Complexes Possessing a Tridentate N-Heterocyclic Carbene Amidate Alkoxide Ligand: Access to Oxygen-Bridging Dimer Structures, Chem. Int. Ed. 47 (48) (2008) 9326–9329.
[41] D. Ćoćić, S. Jovanović, S. Radisavljević, J. Korzekwa, A. Scheurer, R. Puchta, D. Baskić, D. Todorović, S. Popović, S. Matić, New monofunctional platinum (II) and palladium (II) complexes: Studies of the nucleophilic substitution reactions, DNA/BSA interaction, and cytotoxic activity, J. Inorg. Biochem. 189 (2018) 91–102.
[42] R.O. Omondi, R. Bellam, S.O. Ojwach, D. Jaganyi, A.A. Fatokun, Palladium (II) complexes of tridentate bis (benzazole) ligands: Structural, substitution kinetics, DNA interactions and cytotoxicity studies, J. Inorg. Biochem. 210 (2020) 111156.
[43] D. Ćoćić, S. Jovanović-Stević, R. Jelić, S. Matić, S. Popović, P. Djurdjević, D. Baskić, B. Petrović, Homo-and hetero-dinuclear Pt (II)/Pd (II) complexes: studies of hydrolysis, nucleophilic substitution reactions, DNA/BSA interactions, DFT calculations, molecular docking and cytotoxic activity, Dalton Trans. 49 (41) (2020) 14411–14431.
[44] S. Mandal, S.K. Tarai, A. Pan, R. Bhaduri, P. Biswas, S.C. Moi, Cytotoxic effects of Pd (II) complexes on cancer and normal cells: Their DNA & BSA adduct formation and theoretical approaches, Bioorg. Chem. 128 (2022) 106093.
[45] A. Shanmugapriya, R. Jain, D. Sabarinathan, G. Kalaiarasi, F. Dallemer, R. Prabhakaran, Structurally different mono-, bi-and trinuclear Pd (II) complexes and their DNA/protein interaction, DNA cleavage, and anti-oxidant, anti-microbial and cytotoxic studies, New J. Chem. 41 (18) (2017) 10324–10338.
[46] Y. Lu, Z. Hou, M. Li, N. Wang, J. Wang, F. Ni, Y. Zhao, B. Zhang, N. Xi, Increasing the cytotoxicity of Ru (ii) polypyridyl complexes by tuning the electron-donating ability of 1, 10-phenanthroline ligands, Dalton Trans. 51 (42) (2022) 16224–16235.
[47] A. Mondal, U. Sen, N. Roy, V. Muthukumar, S.K. Sahoo, B. Bose, P. Paira, DNA targeting half sandwich Ru (II)-p-cymene-N^ N complexes as cancer cell imaging and terminating agents: Influence of regioisomers in cytotoxicity, Dalton Trans. 50 (3) (2021) 979–997.
[48] R. Bellam, D. Jaganyi, R.S. Robinson, Heterodinuclear Ru–Pt Complexes Bridged with 2, 3-Bis (pyridyl) pyrazinyl Ligands: Studies on Kinetics, Deoxyribonucleic Acid/Bovine Serum Albumin Binding and Cleavage, In Vitro Cytotoxicity, and In Vivo Toxicity on Zebrafish Embryo Activities, ACS Omega (Westport) 7 (30) (2022) 26226–26245.
[49] P. Bera, A. Aher, P. Brandao, S.K. Manna, I. Bhattacharyya, C. Pramanik, B. Mandal, S. Das, P. Bera, Synthesis, structure elucidation and dft study of a new thiazole–pyridine anchored nnn donor and it's cobalt (II) complex: In-vitro antitumor activity against U937 cancer cells, dna binding property and molecular docking study, J. Mol. Struct. 1224 (2021) 129015.
[50] M. Cory, D.D. McKee, J. Kagan, D. Henry, J.A. Miller, Design, synthesis, and DNA binding properties of bifunctional intercalators. Comparison of polymethylene and diphenyl ether chains connecting phenanthridine, J. Am. Chem. Soc. 107 (8) (1985) 2528–2536.
[51] A.A. Franich, M.D. Živković, J. Milovanović, D. Arsenijević, A. Arsenijević, M. Milovanović, M.I. Djuran, S. Rajković, In vitro cytotoxic activities, DNA-and BSA-binding studies of dinuclear palladium (II) complexes with different pyridine-based bridging ligands, J. Inorg. Biochem. 210 (2020) 111158.
[52] I. Mitra, S. Mukherjee, B. Misini, P. Das, S. Dasgupta, W. Linert, S.C. Moi, Synthesis, biological evaluation, substitution behaviour and DFT study of Pd (II) complexes incorporating benzimidazole derivative, New J. Chem. 42 (4) (2018) 2574–2589.
[53] G.K. Mutua, R. Bellam, D. Jaganyi, A. Mambanda, The role of N, N-chelate ligand on the reactivity of (η6-p-cymene) Ru (II) complexes: kinetics, DNA and protein interaction studies, J. Coord. Chem. 72 (17) (2019) 2931–2956.
[54] J. Kljun, I. Bratsos, E. Alessio, G. Psomas, U.k. Repnik, M. Butinar, B. Turk, I. Turel, New uses for old drugs: attempts to convert quinolone antibacterials into potential anticancer agents containing ruthenium, Inorg. Chim. Acta 52 (15) (2013) 9039–9052.
[55] K. Karami, Z.M. Lighvan, S.A. Barzani, A.Y. Faal, M. Poshteh-Shirani, T. Khayamian, V. Eigner, M. Dušek, Design and synthesis of a novel trinuclear palladium (ii) complex containing an oxime chelate ligand: Determining the interaction mechanism with the DNA groove and BSA site I by spectroscopic and molecular dynamics simulation approaches, New J. Chem. 39 (11) (2015) 8708–8719.
[56] A. Abedi, Z.M. Lighvan, S.N. Ostad, Cytotoxicity and DNA/BSA binding ability of copper (II) complexes with dimethylbithiazole, Monatsh Chem. 147 (9) (2016) 1651–1658.
[57] M.M. Milutinović, A. Rilak, I. Bratsos, O. Klisurić, M. Vraneš, N. Gligorijević, S. Radulović, Ž.D. Bugarčić, New 4′-(4-chlorophenyl)-2, 2′: 6′, 2 ″-terpyridine ruthenium (II) complexes: synthesis, characterization, interaction with DNA/BSA and cytotoxicity studies, J. Inorg. Biochem. 169 (2017) 1–12.
[58] Y.P. Zhang, Y. Li, G.C. Xu, J.Y. Li, H.Y. Luo, J.Y. Li, L. Zhang, D.Z. Jia, Synthesis, crystal structure, DNA/bovine serum albumin binding and antitumor activity of two transition metal complexes with 4-acylpyrazolone derivative, Appl. Organomet. Chem. 33 (3) (2019) e4668.
[59] S. Jain, K. Bhar, S. Kumar, S. Bandyopadhyaya, S. Tapryal, C.C. Mandal, A.K. J. Sharma, Homo-and heteroleptic trimethoxy terpyridine–Cu (ii) complexes: synthesis, characterization, DNA/BSA binding, DNA cleavage and cytotoxicity studies, Dalton Trans. 49 (13) (2020) 4100–4113.
[60] M.Z. Koh, W.Y. Ho, S.K. Yeap, N.M. Ali, L. Boo, N.B. Alitheen, Regulation of cellular and cancer stem cell-related putative gene expression of parental and CD44 + CD24− sorted MDA-MB-231 cells by cisplatin, Pharmaceuticals 14 (5) (2021) 391.
[61] T. Kashkoulinejad-Kouhi, S. Safarian, B. Arnaiz, L. Saa, Enhancement of cisplatin sensitivity in human breast cancer MCF-7 cell line through BiP and 14-3-3ζ co-knockdown, Oncol. Rep. 45 (2) (2021) 665–679.
[62] R. Castro-Ramírez, N. Ortiz-Pastrana, A.B. Caballero, M.T. Zimmerman, B. S. Stadelman, A.A. Gaertner, J.L. Brumaghim, L. Korrodi-Gregório, R. Pérez-Tomás, P. Gamez, DNA interactions of non-chelating tinidazole-based coordination compounds and their structural, redox and cytotoxic properties, Dalton Trans. 47 (22) (2018) 7551–7560.
[63] R.E. Rulke, J.M. Ernsting, A.L. Spek, C.J. Elsevier, P.W. van Leeuwen, K. Vrieze, NMR study on the coordination behavior of dissymmetric terdentate trinitrogen ligands on methylpalladium (II) compounds, Inorg. Chem. 32 (25) (1993) 5769–5778.
[64] G.M. Sheldrick, Advances, SHELXT–Integrated space-group and crystal-structure determination, Acta Crystallogr. C: Struct. Chem. 71 (1) (2015) 3–8.
[65] O.V. Dolomanov, L.J. Bourhis, R.J. Gildea, J.A. Howard, H. Puschmann, OLEX2: a complete structure solution, refinement and analysis program, Appl. Cryst. 42 (2) (2009) 339–341.
[66] G.M. Sheldrick, A short history of SHELX, Acta Crystallogr. A: Found. Crystallogr. 64 (1) (2008) 112–122.
[67] R.O. Omondi, D. Jaganyi, S.O. Ojwach, A.A. Fatokun, (Pyridyl) benzoazole ruthenium (III) complexes: Kinetics of ligand substitution reaction and potential cytotoxic properties, Inorg. Chim. Acta. 482 (2018) 213–220.